Photochemical mineralisation in a boreal brownwater lake: Considerable temporal variability and minor contribution to carbon dioxide production

M. M. Groeneveld[1], L. J. Tranvik[1], S. Natchimuthu[2] and B. Koehler[1]

[1]{Ecology and Genetics/Limnology, Evolutionary Biology Centre, Uppsala University, Norbyvägen 18 D, 75236 Uppsala, Sweden}

[2]{Department of Thematic Studies - Environmental Change, Linköping University, 58183 Linköping, Sweden}

Correspondence to: B. Koehler (birgit.koehler@ebc.uu.se)

Abstract

Sunlight induces photochemical mineralisation of chromophoric dissolved organic matter (CDOM) to dissolved inorganic carbon (DIC) in inland waters, resulting in carbon dioxide (CO_2) emissions to the atmosphere. Photochemical rate modelling is used to determine sunlight-induced CO_2 emissions on large spatial and temporal scales. A sensitive model parameter is the wavelength-specific photochemical CDOM reactivity, the apparent quantum yield (AQY). However, the temporal variability of AQY spectra within inland waters remains poorly constrained. Here, we studied a boreal brownwater lake in Sweden. We measured AQY spectra for photochemical DIC production monthly between June and November 2014 and parameterised a photochemical rate model. The total AQY between 280 and 600 nm increased about threefold during the open water period, likely due to a high rainfall event with consecutive mixing in autumn that increased availability of highly photoreactive CDOM. However, the variability in AQY spectra over time was much smaller than previously reported variability in AQY spectra between lakes. Yet, using either the AQY spectrum from the least or from the most photoreactive water sample resulted in a 5-fold difference in simulated annual DIC photoproduction (2012-2014), with 2.0 ± 0.1 and 10.3 ± 0.7 g C m^{-2} yr^{-1}, respectively. This corresponded to 1 and 8% of the mean CO_2 emissions measured from this

lake. We conclude that (1) it may be recommendable to conduct repeated AQY measurements throughout the season for more accurate simulation of annual photochemical DIC production in lakes and (2), in agreement with previous studies, direct CDOM photomineralisation makes only a minor contribution to mean CO_2 emissions from Swedish brownwater lakes.

1 Introduction

Inland waters play a substantial role in carbon cycling (Cole et al., 2007; Battin et al., 2009; Tranvik et al., 2009). The major carbon fluxes occurring in inland waters are burial in sediments and mineralisation followed by carbon dioxide (CO_2) emission into the atmosphere. A substantial fraction of the CO_2 emissions is attributed to microbial mineralisation of dissolved organic carbon (DOC) (del Giorgio et al., 1997; Duarte and Prairie, 2005). Also, sunlight contributes to CO_2 production via photochemical mineralisation of chromophoric dissolved organic matter (CDOM) (Granéli et al., 1996; Bertilsson and Tranvik, 2000). According to the first global upscaling study, up to about one tenth of the CO_2 emissions from lakes and reservoirs are directly sunlight induced (Koehler et al., 2014). However, the importance of sunlight for carbon processing varies strongly between systems and studies (Granéli et al., 1996; Molot and Dillon, 1997; Ziegler and Benner, 2000; Cory et al., 2014).
Measuring photochemical DOC mineralisation, equivalent to photochemical production of dissolved inorganic carbon (DIC), in the field is challenging and seldom conducted (Salonen and Vähätalo, 1994; Graneli et al., 1996). Photochemical rate modelling is used to obtain DIC photoproduction estimates at large spatial and temporal scales. Model parameterisation requires wavelength-specific irradiance, CDOM absorbance, attenuation and photochemical CDOM reactivity, i.e. the apparent quantum yield (AQY) defined as DIC produced per mol photons absorbed (Fichot and Miller, 2010; Koehler et al., 2014). The AQY is a sensitive model parameter but until now spectra have only been published from a small number of lakes (Vähätalo et al., 2000; Vähätalo & Wetzel, 2004; Koehler et al., 2014; Cory et al., 2014; Vachon et al., 2016), and temporal variability of AQY spectra within individual systems is even less studied (Cory et al., 2014; Vachon et al., 2016). Given the limited knowledge on spatial and temporal variability of AQY spectra the first large-scale modelling study of photochemical CDOM mineralisation in inland waters assumed that AQY spectra determined

for single systems and on single occasions represented photochemical reactivity on larger spatial and temporal scales (Koehler et al., 2014).

However, temporal variability in AQY spectra is to be expected. For example, photochemical DIC production can increase with increasing CDOM aromatic content, increasing iron concentrations or decreasing pH (Gao and Zepp, 1998; Bertilsson and Tranvik, 2000; Anesio and Granéli 2004; Stubbins et al., 2010). An important process that may influence CDOM quality on a seasonal scale is photobleaching, where CDOM is transformed to less coloured and less aromatic compounds (Brinkmann et al., 2003; Müller et al., 2014). Consequently, CDOM can become less photoreactive after light exposure (Lindell et al., 2000; Gonsior et al., 2013), and this "light dose dependence" may be especially important at high latitudes (Zhang et al., 2006). Temporal fluctuations may also be caused by photoreactive terrestrial CDOM entering aquatic systems through heavy rainfall and runoff (Spencer et al., 2010; Hughes et al., 2013). For example, studies in a tropical systems observed the largest and smallest photochemical mineralisation rates during rainy and dry season, respectively (Amado et al., 2006; Suhett et al., 2007).

In this study, we examined temporal variability in photochemical reactivity and photochemical DIC production in a small brownwater lake in Sweden. We then evaluated differences in photochemical DIC production simulated using a photochemical rate model with time-constant vs. repeatedly measured AQY spectra. Finally, we assessed the contribution of mean annual photochemical DIC production to total mean CO_2 emission from this lake.

2 Material and methods

2.1 Study lake and sampling

Erssjön (58°37′ N, 12°16′ E) is a small brownwater lake (59 997 m^2, mean depth 1.3 m, maximum depth 4.4 m) in the Bäveån catchment in southwest Sweden (Fig. 1a). The lake is mostly surrounded by forest, mainly spruce and birch, and some agricultural land, and is part of the Skogaryd Research Site (Klemedtsson et al., 2010). In 2014, the ice disappeared from lake Erssjön on 25 February (S. Peter, personal communication, 2014) and the lake remained ice-free until 31 December. For this study, 2L of surface water was grab-sampled into acid-

washed polyethylene bottles in the middle of the lake, monthly between April and November 2014. The samples were kept dark and cold (<10°C) until and during transport to Uppsala University within one to three days. Upon arrival, the water was filtered sequentially through pre-combusted glass fibre filters (Whatman GF/F, GE Healthcare, Little Chalfont, Buckinghamshire, UK) and 0.2 µm polyethersulfone membrane filters (Supor®-200, Pall Corporation, Ann Arbor, Michigan, USA) into glass bottles. Filtration through the 0.2 µm membrane filters, which was conducted to minimise microbial abundance and hence microbial respiration during the irradiation experiments (Sect. 2.3), reduced the integrated CDOM absorbance between 300 and 600 nm by 4.4% compared to that of GF/F filtrate. The samples were wrapped in aluminium foil and kept at 4°C until further analysis within three weeks.

2.2 Chemical and optical water properties

DOC concentrations were measured with a total carbon analyser (Shimadzu TOC-L, Shimadzu Corporation, Kyoto, Japan), as non-purgeable organic carbon (NPOC) concentration. UV-Vis absorbance spectra (200 to 600 nm) of filtered water were measured in a 1 cm quartz cuvette using a Lambda35 UV-VIS Spectrometer (PerkinElmer Lambda 25, Perkin Elmer, Waltham, USA). Based on the Beer–Lambert law, absorption coefficients a (m^{-1}) were calculated as:

$$a = \frac{A \ln 10}{L} \quad (1)$$

where A is absorbance (dimensionless) and L is optical path length (m) (Kirk, 2010). The specific UV absorption coefficient at 254 nm ($SUVA_{254}$; L mg C^{-1} m^{-1}), a commonly used indicator of DOC aromaticity (Weishaar et al., 2003), was calculated as the ratio between a_{254} and the DOC concentration ($mgCL^{-1}$). Synchronous fluorescence scans were obtained using a FluoroMax-4 Spectrofluorometer (FluoroMax-4, Jobin Yvon, Horiba, Kyoto, Japan), with excitation-emission matrices (EEMs) between excitation wavelengths 250 to 445 nm with 5 nm increments, and emission wavelengths 300 to 600 nm with 4 nm increments. The EEMs were blank-subtracted using a sample of Milli-Q water run on the same day, corrected for instrument biases and inner filter effects and normalised to Raman units (Lawaetz and Stedmon, 2009; Kothawala et al., 2013). Three commonly used indices were calculated at fixed excitation/emission wavelength pairs or regions (Coble et al., 2014; Gabor et al., 2014).

All fluorescence corrections and analyses were performed using the FDOMcorr toolbox for MATLAB (Murphy et al., 2010).

For total nitrogen (TN) analysis, all nitrogen species were oxidised to nitrate using potassium persulfate and sodium hydroxide at high pressure and temperature in an autoclave. TN was determined spectrophotometrically by subtracting a blank and absorbance at 275 nm from absorbance at 220 nm (PerkinElmer Lambda 40 UV- VIS spectrometer, Perkin Elmer, Norwalk, CT, USA). EDTA (disodium-dyhydrogen- ethylendiamine-tetraacetat) was used for the calibration curve (Rand et al., 1976). Total phosphorus (TP) was converted to orthophosphate using oxidative hydrolysis with potassium persulfate in acid solution at high pressure and temperature in an autoclave, and to phosphorus molybdate by reaction with ammonium molybdate, which was then reduced with ascorbic acid, accelerated by antinome. The samples were analysed spectrophotometrically at 882 nm as molybdate reactive phosphorus (PerkinElmer Lambda 40) (Menzel and Corwin, 1965; Murphy and Riley, 1958). TP concentrations measured for the LAGGE project were used (M. Wallin, unpublished data).

2.3 Apparent quantum yield

The wavelength-specific CDOM reactivity towards photochemical DIC production, i.e. the apparent quantum yield (AQY) defined as mol DIC produced per mol CDOM absorbed photons, was determined monthly between June and November 2014 similarly as described in Koehler et al. (2014). The measurements from April and May could not be used due to failure of the DIC analyser. Specifically, to minimise initial DIC concentration, the samples were acidified (10 % HCl to pH < 3), bubbled with nitrogen gas for 25 min to remove the CO_2, and re-adjusted to the original pH using 1M NaOH. The amount of HCl and NaOH added never exceeded 0.5 % of the sample volume. The water was re-filtered with 0.2µm Supor®-200 filters to minimise bacterial abundance and hence respiration during subsequent irradiation. During this filtration step the water, in which oxygen concentrations were reduced during bubbling with N_2, was also aerated again. The water was then filled into cylindrical glass vials with flat quartz top (50 mL volume; Fig. S1). The incubation vials were soaked in 10 % HNO_3 for at least ten hours and rinsed thoroughly with Milli-Q water before and after each experiment. To systematically manipulate the irradiance field, cut-off filters (CVI Laser Corporation, obtained from former Gamma Optronik AB, Sweden and Oriel Instruments,

Newport Corporation, Irvine, California) that cut off irradiance with wavelengths below 455, 420, 380, 350, 320, 309 or 280 nm (Fig. S1) were placed on top of the vials. All filters and dark controls, where a black lid was attached to the vial, were used in triplicate. Thin needles were inserted through the septa covering one of the vial outlets to enable pressure release during irradiation in the solar simulator. Using three vials with and three vials without a needle through the septum, which were filled with a standard of 1500 ppb IC and left at room temperature for 24 h, we verified that this did not affect DIC concentration in the vessel (p = 0.113). Then, the samples were irradiated for five hours using a solar simulator (Q-Sun 1000 Xenon test chamber, Q-panel Lab Products Europe, Bolton, UK) set to 0.59 W m^{-2} at 340 nm (calibrated with the instrument's CR20 Calibration Radiometer). During irradiation, the samples were standing in a cooled water bath, maintaining the temperature around the vials at approximately 25°C. Initial and final DIC concentrations were measured from each vial with the Shimadzu TOC-L analyser, and the photochemical DIC production in each vial was calculated as the difference between the final and initial DIC concentration, minus the mean production in the dark controls. A calibration curve was created before each run, using the auto-dilution function to create six standards of different concentrations from a 5 or 10 ppm solution that was freshly prepared from a 1000 ppm IC stock solution ($R^2 \geq 0.998$) (Shimadzu user manual). DIC concentrations were measured in a minimum of five injections of 150 µL, resulting in SD < 0.5 ppb and/or CV < 2%. In the June experiment the "dark DIC production" was −0.2 to −17 ppb. We suspect this was due to a slight offset in the calibration of the instrument during the measurements and/or difficulty to detect very low DIC concentrations, and set the control values to zero. In the August experiment, the dark production of one control set was considerably higher than usual. Since the acid-washing step had been missed during cleaning of these three vessels we suspect the high concentrations were caused by contamination. Therefore, the values of the other control set were used for calculating photochemical DIC production. This affected the resulting AQY spectrum only to a minor extent (Fig. S2b in the Supplement). Across experiments, DIC production in the dark controls averaged 26.2 ± 4.6 ppb, corresponding to 3 and 24% of the average DIC production under the 250 and 455 nm cut-off filter, respectively. On eight occasions throughout the study period, irradiance spectra (280–600 nm) were measured at the location of each vial using a spectrometer (BLACK Comet UV-VIS, StellarNet Inc., Tampa, Florida, USA) equipped with

a fibre optic cable (STEF600-UVVis-SR, StellarNet) and a cosine receptor for UV-Vis near-infrared irradiance (STE-CR2, StellarNet). Absorbed photons were calculated accounting for the inner filter effect (Hu et al., 2002). The calculated number of CDOM-absorbed photons was in good agreement with CDOM-absorbed photons determined using nitrite ultraviolet actinometry, where the photon exposure of an irradiated sample is quantified from the photochemical production of salicylic acid formed during reaction of the hydroxide radical with benzoic acid (Jankowski et al., 1999; Jankowski et al., 2000). The response bandwidth was verified, and the photoproduced salicylic acid was detected using fluorescence spectrophotometry (SPEX FluoroMax-4; Jankowski et al., 1999). CDOM-absorbed photons determined with the spectrally resolved calculation used during AQY determination and the broadband actinometry differed by a factor of 1.43 ± 0.04 under the complete irradiance spectrum in the solar simulator.

AQY spectra were calculated using weighted parameter optimisation (Rundel, 1983) to an exponential function

$$\Phi = e^{-(m_1+m_2(\lambda-290))} \quad (2)$$

where Φ is the AQY of DIC photoproduction (mol DIC mol photons^{-1}), λ is the wavelength (nm) and m_1 and m_2 are fit parameters (Johannessen and Miller, 2001), using the Nelder Mead simplex minimisation algorithm (Nelder and Mead, 1965) implemented in the function *optim* in R 3.1.0 (R Development Core Team, 2014), and using a set of different starting values to verify stability of the solution. The total AQY (AQY_{total}) was calculated using the DIC production measured under full irradiance (280 nm filter) divided by CDOM-absorbed photons integrated from 280 to 600 nm. For uncertainty estimation we used bootstrapping (Ritz and Streibig, 2008; Crawley et al., 2012), where we resampled the monthly measured photochemical DIC production with replacement (6000 times), assigned the respective CDOM-absorbed photons, fitted AQY spectra to each bootstrap dataset. We give the 2.5% and 97.5% quantiles of the resulting bootstrap distribution of parameter estimates as 95% confidence intervals. Kernel density estimation was used to estimate the probability density function for the bootstrap distributions of parameter estimates. To obtain simultaneous pointwise confidence intervals (Fig. 2) we used the 6000 bootstrap parameter estimates to predict the AQY at five discrete wavelengths, about midway between the cut-off filters used

during the irradiation experiments (295, 330, 365, 400 and 435 nm). The confidence level was Bonferroni-corrected to reduce the family-wise type I error rate according to $(1 - \frac{\alpha}{n}) \cdot 100\%$, where α is the significance level and *n* is the number of simultaneous calculations.

To statistically test the temporal variability in AQY we calculated the difference in the discrete AQY values calculated above between adjacent sampling months (i.e. comparing June to July, July to August, etc., including November to June). Again, the confidence level was adjusted for multiple testing using the Bonferroni correction. A temporal difference (*p*-value ≤ 0.05) exists when the obtained 95% confidence intervals of the differences between adjacent months exclude zero in at least one case.

2.4 In situ photochemical DIC production

During 23 to 25 July 2014, we determined in situ photochemical DIC production rates similarly as described in Granéli et al., 1996. Specifically, we filled filtered lake water (0.2 µm membrane filters) into quartz tubes (38 mL, 2 cm diameter) and corresponding borosilicate dark control tubes wrapped in aluminium foil. Three quartz and two to three dark tubes were attached horizontally to steel wire racks, which were secured to a floating wooden frame that was kept in place with two anchors. This setup was duplicated and the two frames were positioned in the lake at least 50 m from the shoreline (Fig. 1b; red dots). The racks with the tubes were positioned such that the centre of the tubes was positioned at 1, 4 and 8 cm water depth and well within the frame, so that no shading occurred (Fig. 1c). During the 2 day incubation period the anchors sank into the sediment and pulled the frames down by approximately 1 cm. After incubation, all tubes were wrapped in aluminium foil, placed with cooling blocks in cooling boxes for transport, and stored at 4°C until analysis at Uppsala University within two days. Initial DIC concentration was measured from one water sample taken and filtered at the start of the incubation as described above, and kept cold and dark until analysis after three days. Final DIC concentrations were measured directly from the incubation tubes and averaged for the three pseudoreplicate tubes. In one case the measured value of one of the dark triplicates was about 35% higher than all other dark values. This sample was considered to be contaminated and excluded from the calculations. The DIC production at the different water depths was then calculated as the mean of the two set-ups and standardised to mg C m^{-3} d^{-1}.

2.5 Photochemical rate modelling

Using photochemical rate modelling (Eq. 3), DIC photoproduction was simulated for the open water periods of 2012 to 2014 as:

$$\boldsymbol{\Psi_{DIC}^{day} = \int_{\lambda_{min}}^{\lambda_{max}} E_{od}^{day}(\lambda, 0^-) a_g(\lambda) e^{-(K_d(\lambda)z)} \phi(\lambda) d\lambda} \quad \text{(eq. 3)}$$

The model calculates the daily photochemical DIC production rate (Ψ_{DIC}^{day}, mol C $m^{-3} d^{-1} nm^{-1}$) over water depth (z, m) based on daily-integrated downwelling scalar irradiation just below the water surface ($E_{od}^{day}(\lambda,0^-)$, mol photons m^{-2} d^{-1} nm^{-1}), CDOM absorption coefficient (a_g, m^{-1}), vertical attenuation coefficient for downwelling irradiance (K_d, m^{-1}) and the apparent quantum yield ($\Phi(\lambda)$, mol DIC mol photons^{-1}) over the photochemically relevant wavelength range (λ, 280–600nm) (Fichot et al., 2010; Koehler et al., 2014). Daily-integrated clear-sky irradiance spectra were obtained using the libRadtran model (version 1.6) for radiative transfer (Mayer et al., 2005), parameterised and cloud corrected as described in Koehler et al. (2014). For the year 2014, for which monthly AQY spectra were measured between June and November, we used four different AQY parameterisations and assessed their influence on the simulated photochemical DIC production. In the first parameterisation, we assumed that the measured AQY and absorbance spectra were representative for one month around the sampling dates. The spectra measured in June were also used for the open-water period prior to June, and the spectra measured in November were used until the end of the open water period in December. In the second parameterisation, we assumed that the AQY spectrum fitted through all data points obtained between June and November is a representative description of the photochemical reactivity in the lake. The absorbance spectra were again used for one month around the sampling dates. In the third and fourth parameterisation, we assumed that the observed most and least photoreactive water sample was representative throughout the whole open water period, respectively.

$SUVA_{254}$ was calculated for the years 2012 to 2014, using data from this study as well as absorbance spectra and TOC concentrations measured in 2012 and 2013 (M. Wallin, unpublished data). Since no actual ice-on and ice-off dates were available for lake Erssjön in 2012 and 2013, the long-term average (1970–2007) ice-cover dates for the nearby (19 km) lake Ellenösjön were used (3 April to 7 December; SMHI, 2013).

We also compared simulated photochemical DIC production with the in situ measured rates. In order to compare with the rates measured in the incubation tubes, we integrated the simulated sunlight-induced DIC production rates over the respective depth intervals and for the same time period as the in situ measurement. Since the duration of the incubation was only two days, hourly rather than daily irradiance spectra were used. We assumed that the quartz tubes did not interfere with irradiance. While, in reality, the quartz tubes will affect the number and optical path length of the photons entering the tube we considered this effect minor compared to other uncertainties during the in-situ measurements (see Discussion). The absorbance coefficients and apparent quantum yield were obtained from water sampled on the last day of the incubation (the July sample of this study, Fig. 1).

2.6 Total CO_2 emissions

Total CO_2 emissions from the lake surface were measured using plastic floating chambers of volume 6.3 L and area 0.07 m^2, which were covered with aluminum tape to reflect sunlight thereby minimising internal heating, equipped with Styrofoam collars to enable floating and anchored to the lake bottom. The chamber walls extended 3 cm into the water on deployment. Mini CO_2 sensors (CO_2 Engine® ELG, SenseAir AB, Sweden; measuring range 0-10000 ppm) were fitted inside the chamber and programmed to log CO_2 concentrations every 5 minutes (Bastviken et al., 2015). Three chambers were deployed over water depths of 0.5, 2.5 and 4 m (Fig. 1b; white dots). Before flux measurements, the chambers were vented using a 20 cm long PVC tube fitted with a 3-way luer-lock stopcock (Becton-Dickinson, USA). After venting, the chambers were closed for 30 minutes, and the rate of change in CO_2 concentration inside the chamber was calculated using linear regression. When the change of CO_2 concentrations over time was nonlinear, with $R^2 < 0.9$, we discarded the time series. The rates were converted to moles using the ideal gas law and divided by area and time to obtain emissions. Measurements were made approximately every two weeks during June to October 2012 and April to November 2013. During each visit, emissions were measured on two consecutive days.

2.7 Statistical analyses

Two sample *t* tests were used to test for differences between DIC production under the cut-off filters and the dark controls, and to compare DIC concentrations in the incubation vials with

and without a needle through the septum. Linear mixed effects models were used to test for changes in the total AQY, the AQY fit parameters and the chemical and optical water properties over time. The R^2 of a linear least squares regression between DIC photoproduction observed under the cut-off filters and predicted using the fitted AQY spectrum as well as the normalised root mean squared error was used to assess performance of the fitted AQY spectra to reproduce the observations. In all statistical tests, differences were considered significant if *p-value* < 0.05. Mean values are reported with ±1 standard error. Analyses were conducted using R 3.1.0 (R Development Core Team, 2014).

3 Results

3.1 Chemical and optical water properties

Water chemical and optical properties were similar in lake Erssjön from April to July 2014 (Table 1; Fig. S2a). Sampling in August was preceded by a period of high rainfall with 46 mm precipitation within seven days. This corresponded to almost 5% of the annual rainfall in 2014, and another 97 mm precipitation was observed during the remainder of the month (SMHI, 2015). Subsequently, from August until November, DOC concentrations and absorbance coefficients were approximately 50% higher than earlier in the year (p_{DOC} = 0.022, p_{a254} = 0.009, p_{a420} = 0.025), while pH and $SUVA_{254}$ remained similar. TN and TP were similar across the open-water period with the exception of August, when TN was approximately twice as high. The fluorescence index (FI) increased slightly throughout the study period (P = 0.003) whereas the freshness index ($\beta : \alpha$) showed no apparent pattern over time. The humification index (HIX) decreased in spring and early summer, increased towards autumn and then decreased again (Table 1). DOC concentrations, a_{420} and $SUVA_{254}$ were similar during 2012–2014 (Table 2).

3.2 Apparent quantum yield

The DIC production under full irradiance (p = 0.002) and the AQY_{total} (p = 0.008) increased throughout the sampling year, while there was no significant change in CDOM-absorbed photons (Table 3). The monthly AQY spectra, evaluated at five discrete wavelengths and tested simultaneously, differed from each other (p < 0.05; Fig. 2). Specifically, while the AQY fit parameter m_1 did not change throughout the sampling period, the slope parameter m_2 decreased over time (p = 0.005; Table 3). This is also illustrated by the density of the bootstrap

distribution of parameter estimates. The densities of m_1 overlapped for all months (Fig. S2c), while, for example, the densities of m_2 for June and July did not overlap with the densities of October and November (Fig. S2d). For each measurement, the fitted AQY spectra reliably predicted the observations, with R^2 of a linear regression between observed and predicted DIC photoproduction ≥ 0.96, slopes close to unity and *n*RMSE ≤ 7% (Table 3).

3.3 Observed vs. simulated photochemical DIC production rates

The in situ photochemical DIC production rates decreased sharply by about a factor of five from just below the water surface to 4 cm water depth (Fig. 3, black numbers). At 8 cm depth, DIC production did not differ between the irradiated and the dark tubes, i.e. the photochemical DIC production was below the detection limit. The simulated photochemical DIC production also decreased sharply with increasing water depth (Fig. 3, red curve). When assuming that the experimental tubes remained at the intended depth of incubation, the simulated photochemical DIC production differed by 114% at 1 cm and by 22% at 4 cm from the observed rates, and, in accordance with the measurements, was small at 8 cm depth (Fig. 3, red numbers). However, the racks to which the tubes were attached were pulled down by approximately 1 cm over the course of the two-day incubation period as their anchors sank into the sediment. If the depth intervals of integration are taken to be 1 cm lower than the intended depths, the simulated DIC photoproduction rates differed by 38% at 2 cm and by 9 % at 5 cm from the observed values (Fig. 3, red numbers in parentheses).

3.4 Photochemical rate modelling

To assess which AQY spectrum was most representative for the photochemical reactivity observed throughout the open-water period of 2014 we used the monthly AQY spectra as well as the pooled AQY spectrum to predict the DIC photoproduction observed in all six irradiation experiments. This revealed that the AQY spectra of the more photoreactive water samples (October and November) gave the best prediction, considerably better than the pooled AQY spectrum, which according to this evaluation underestimated the observed DIC photoproduction (Table 3). We therefore used the AQY spectrum from the most photoreactive water sample (November) in photochemical rate modelling for the year 2014, which gave a simulated DIC photoproduction of 12.2 g C m^{-2} y^{-1} (Table 3, Fig. S3a). Using the AQY spectrum from the least photoreactive water sample (July) for annual simulation the estimate

would be 5.6-fold smaller (Table 3, Fig. S3b), and using the monthly measured AQY spectra for periods of one month around the sampling date the estimate would be three times smaller (Table 3; Fig. S3c). The rather small estimate when using the monthly measured AQY spectra for month-long time periods is related to the facts that 1) the comparatively small photochemical reactivity measured during the first sampling in June was used to simulate photochemical mineralisation also for the open-water period prior to June and 2) observed photochemical reactivity was smallest during summer when irradiance is maximal, and highest during late autumn when irradiance is low (Table 3, Fig. S3d).

CDOM absorbance, as well as $SUVA_{254}$ and DOC concentrations, were similar throughout 2012 to 2014 (Table 2). Therefore, we assumed that photoreactivity was similar as observed in 2014 and also used the least and most productive AQY spectra measured in 2014 to simulate photochemical DIC production for the years 2012 and 2013, in combination with the measured absorbance spectra and simulated irradiance. Interannual variability in irradiance was very small (Fig. 4a) and hence, in combination with similar CDOM absorbance and the assumption that photoreactivity was similar as in 2014, simulated DIC photoproduction was similar across the years (Table 2; Fig. 4b). Simulating irradiance over the years 2004 to 2014 showed that the irradiance that lake Erssjön received in 2012 to 2014 was representative for the decadal mean ($4.10 \times 10^5 \pm 0.15 \times 10^5$ Wh m^{-2} yr^{-1}). During simulations we assumed that irradiance was not transmitted into the water column during the ice-covered period. If we instead would assume that the ice fully transmits irradiance or ice cover was absent, the yearly simulated photochemical DIC production would increase by 11 to 14%.

4 Discussion

The apparent quantum yield (AQY) spectra for photochemical DIC production, measured monthly between June and November 2014 in a boreal brownwater lake, showed considerable seasonal variability, with the slope of the spectrum decreasing over the open-water season. Photochemical DIC production, simulated using photochemical rate modelling, made a minor contribution to the total CO_2 emissions observed from the same lake (Fig. 5). Hence, similar results from earlier studies in boreal Sweden (Jonsson et al., 2001; Koehler et al., 2014; Chmiel et al., 2016) were corroborated when considering temporal variability in photochemical reactivity as well as in total lake CO_2 emissions. Moreover, the good match

between photochemical DIC production observed in situ and simulated rates (Fig. 2) supported that photochemical rate modelling is a suitable approach to investigate photochemical DOM mineralisation in lakes and its contribution to carbon cycling on broader temporal and spatial scales. This highlights the potential to use a similar method for studying this process also in other climate zones, e.g. for tropical lakes, where the role of photochemical mineralisation for lake carbon cycling remains even less constrained than in boreal and temperate systems.

The DIC photoproduction rates observed in situ in the studied boreal brownwater lake (Fig. 3) were comparable to rates in a Norwegian dystrophic lake (100 and 40mgC m^{-3} d^{-1} at 1 and 10 cm depth, respectively; Salonen and Vähätalo, 1994), five Swedish lakes (100–300 mg C m^{-3} d^{-1} at 1 cm depth; Granéli et al., 1996), and in a Finnish humic lake (300 and 180 mg C m^{-3} d^{-1} at 1 and 2.5 cm depth, respectively; Vähätalo et al., 2000). However, it is difficult to accurately measure DIC photoproduction rates in situ. Wind and wave action make it hard to exactly measure, adjust and stabilise the tubes at the intended depths of incubation. This is especially relevant in the case of a brownwater lake like Erssjön, where DOC photomineralisation is confined to the upper centimetres of the water column and photochemical rates decrease rapidly with increasing water depth (Fig. 3; Granéli et al., 1996; Vähätalo et al., 2000; Koehler et al., 2014). Nevertheless, the simulated and observed DIC photoproduction rates were similar (Fig. 3), giving confidence in the model parameterisation. Given the experimental difficulties, photochemical rate modelling is an attractive method for estimating photochemical DOC mineralisation, especially on large temporal and spatial scales.

The wavelength-specific photochemical reactivity is a critical and sensitive parameter in photochemical rate modelling (Fichot & Miller, 2010; Koehler et al., 2014; Cory et al., 2014). However, knowledge on its variability remains scarce. So far, AQY spectra for photochemical DIC production have only been reported for a small number of Arctic, boreal and temperate lakes (Vähätalo et al., 2000; Vähätalo and Wetzel, 2004; Koehler et al., 2014; Cory et al., 2014; Vachon et al., 2016). Information about temporal variability in AQY spectra across seasons within single lakes is even more rare, with only two studies so far where lake AQY spectra were repeatedly determined during the open-water season (Cory et al., 2014; Vachon et al., 2016). In this study, the AQY spectra determined monthly in a boreal brownwater lake showed a decrease in slope (fit parameter m_2, eq. 2) from June to November (Table 3; Fig.

S2b,d in the Supplement). This suggests that the longer wavelengths contributed more to DIC photoproduction later in the season. However, the variability in AQY spectra over time (CV = 0.11 at λ_{300}) was much smaller (Fig. 1b) than the variability in AQY spectra between lakes of differing CDOM quality and quantity reported so far (CV = 0.52 at λ_{300}; Vähätalo et al., 2000; Vähätalo and Wetzel, 2004; Koehler et al., 2014; Vachon et al., 2016; AQY_{300} of Toolik Lake from June 29, 2012, R. Cory, personal communication, 2014). Yet, given the high sensitivity of simulated DIC photoproduction towards both magnitude and slope of the AQY spectrum, applying AQY spectra measured at different times to the whole open-water period of 2014 resulted in up to 5.6-fold differences in simulated annual DIC photoproduction. Hence, depending on scale and scope of the study as well as feasibility, it may be recommendable to conduct repeated measurements of AQY spectra throughout the season for more accurate simulation of annual photochemical DIC production in lakes, as recently conducted in studies in the Arctic (Cory et al., 2014) and northern temperate and boreal Canada (Vachon et al., 2016).

While photobleaching is a relevant process regulating CDOM absorption on a seasonal scale in some humic boreal lakes (Müller et al., 2014), we did not observe net photochemical bleaching with a potentially associated reduction in DOM photoreactivity (Lindell et al., 2000). However, AQY spectra were only determined from June onwards, leaving the spring, in which photoreactivity may be high (Gonsior et al., 2013; Vachon et al., 2016) and bleaching most prevalent (Lindell et al., 2000; Zhang et al., 2006; Gonsior et al., 2013), unstudied. Values for the fluorescence index were around 1.3 throughout the season, indicating that the fluorescent DOM was mostly of terrestrial origin. Also the freshness index was stable, suggesting no major temporal changes in the proportion of recently produced fluorescent DOM from microbial origin (Gabor et al., 2014). A marked increase in DOC concentrations and absorbance in autumn (Table 1; Fig. S2a in the Supplement) was preceded by a high rainfall event (SMHI, 2015) and consecutive mixing of the lake (S. Peter, personal communication, 2014). Consistent with the observed simultaneous increase in the humification index (Table 1), this event likely added a substantial amount of humified material to the lake, both from land and from the bottom water of the lake itself (Spencer, 2010; Gonsior et al., 2013; Hughes et al., 2013). Hence, rainfall events, mixing of the lake and potentially a shorter residence time towards autumn may have added fresh and more

photoreactive material to the lake. Possibly, this masked photobleaching while increasing photoreactivity (Fig. 2). Similarly, rainfall and input of fresh terrestrial material increased CDOM photoreactivity in tropical lakes (Amado et al., 2006; Suhett et al., 2007). For tropical systems, which receive an even dose of sunlight throughout the year, the importance of photochemical reactivity in regulating temporal variability in photochemical DIC production may be expected to be higher than in boreal lakes, where temporal changes in photochemical reactivity interact with the pronounced seasonality in irradiance. Accordingly, CDOM photoreactivity and irradiance explained a similar amount of variability in photochemical mineralisation across seasons for three boreal and northern temperate lakes (Vachon et al., 2016).

Considering that photoreactions are constrained to a shallow top layer of the lake, the relative contribution of photochemistry to overall dynamics of DOC is uncertain. To address this, we compared the DIC photoproduction with the total CO_2 emissions that were measured from the lake. Assuming that all photoproduced DIC was emitted as CO_2 to the atmosphere, the mean simulated DIC photoproduction ($7.9 \pm 0.3 – 41.3 \pm 2.9$ mg C m^{-2} d^{-1}; 2012–2014) contributes 1 – 8% to the mean observed CO_2 emissions of 562.2 mg C m^{-2} d^{-1} (Fig. 5). Hence, the results of this detailed study in one Swedish brownwater lake are in agreement with a large-scale modelling study for 1086 Swedish lakes, in which the contribution of mean annual DIC photoproduction to CO_2 emissions was about 12% (Koehler et al., 2014). Also in agreement, direct photo-oxidation contributed about 7% to the total DOC mineralisation in a large humic lake in northern Sweden (Jonsson et al., 2001), and 6% in a small brownwater lake in central Sweden (Chmiel et al., 2016). In a study based on 21 463 observations from lakes across Sweden, CO_2 emission ranged from 31.9 to 88.3 g C m^{-2} yr^{-1} (Humborg et al., 2010). Comparing our low and high estimate of simulated DIC photoproduction to these numbers would suggest a directly sunlight-induced contribution of 2 to 6% and 12 to 32% to the total CO_2 emission, respectively. Besides the here studied direct effect of sunlight on DOC mineralisation, sunlight can also stimulate bacterial respiration by partially photo-oxidising DOC. The magnitude of this indirect effect can be as large as that of the direct effect (Lindell et al., 1995; Molot and Dillon, 1997; Bertilsson and Tranvik, 1998; Cory et al., 2014), resulting roughly in a doubling of the estimates presented here. We conclude that the contribution of sunlight to the CO_2 emissions from the studied Swedish brownwater lake was

small. This was also the case when taking temporal variability of AQY spectra into account. Even when using the AQY spectrum from the most photoreactive water sample for annual simulation and considering photostimulation of DOC mineralisation, the contribution of DOC phototransformations to the in-lake carbon cycling would still be minor.

The Supplement related to this article is available online at doi:10.5194/bgd-12-17125-2015-supplement.

Author contributions. B. Koehler designed the study. M. Groeneveld conducted laboratory and field experiments assisted by B. Koehler and L. Tranvik. M. Groeneveld and B. Koehler conducted photochemical rate modelling and data analysis. S. Natchimuthu conducted the total CO_2 flux measurements and analysed the flux data. M. Groeneveld wrote the manuscript with contributions and revision by B. Koehler, L. Tranvik and S. Natchimuthu.

Acknowledgements. All data used for calculation of apparent quantum yield spectra and photochemical rate modelling are available upon request from the corresponding author. This study was funded by the Swedish Research Council for Environment, Agricultural Sciences and Spatial Planning (FORMAS) as part of the research environment "The Color of Water" (grant 2009-1350-15339-81) and by the Swedish Research Council (grant 2011-3475-88773-67). The fieldwork was conducted at and with support from the Skogaryd Research Catchment station, which is a part of SITES (Swedish Infrastructure for Ecosystem Science). As such it was sponsored by the Swedish research council FORMAS as a part of the project Landscape Greenhouse Gas Exchange (LAGGE). We thank L. Klemedtsson and D. Allbrand for organisation and help with water sampling, J. Johansson, C. Bergvall and A. Nilsson for help in the laboratory and/or field, W.L. Miller and L.C. Powers for advise concerning actinometry, Y. Gu for performing the actinometry, R. Larsson for advise concerning calculation and testing of simultaneous pointwise confidence intervals, D. Kothawala for advise concerning fluorescence analysis, D. Bastviken, M. Wallin, S. Peter, K. Einarsdóttir and T. Hilmarsson for sharing advice and/or data. We also thank A. Amado, R. Cory and two anonymous reviewers for their constructive advice on the manuscript.

References

Amado, A. M., Farjalla, V. F., de A. Esteves, F., Bozelli, R. L., Roland, F. and Enrich-Prast, A.: Complementary pathways of dissolved organic carbon removal pathways in clear-water

Amazonian ecosystems: photochemical degradation and bacterial uptake. FEMS Microbiol. Ecol. 56, 8-17, 2006.

Anesio, A. M. and Granéli, W.: Photochemical mineralization of dissolved organic carbon in lakes of differing pH and humic content, Arch. Hydrobiol., 160, 105–116, 2004.

Bastviken, D., Sundgren, I., Natchimuthu, S., Reyier, H. and Gålfalk, M.: Technical Note: Cost-efficient approaches to measure carbon dioxide (CO_2) fluxes and concentrations in terrestrial and aquatic environments using mini loggers, Biogeosciences, 12, 3849-3859, 2015.

Battin, T. J., Luyssaert, S., Kaplan, L. A., Aufdenkampe, A. K., Richter, A., and Tranvik, L. J.: 2009, the boundless carbon cycle, Nat. Geosci., 2, 598–600, 2009.

Bertilsson, S. and Tranvik, L.: Photochemical transformation of dissolved organic matter in lakes, Limnol. Oceanogr., 45, 753–762, 2000.

Brinkmann, T., Sartorius, D., and Frimmel, F. H.: Photobleaching of humic rich dissolved organic matter, Aquat. Sci., 65, 415–424, 2003.

Chmiel, H. E., Kokic, J., Denfeld, B. A., Koehler, B., Einarsdottír, K., Wallin, M. B., Isidorova, A., Bastviken, D., Ferland, M., and Sobek, S.: The role of sediments in the carbon budget of a small boreal lake, Limnol. Oceanogr., accepted, 2016.

Coble, P. G., Spencer, R. G. M., Baker, A., and Reynolds, D. M.: Aquatic organic matter fluorescence, in: Aquatic Organic Matter Fluorescence, edited by: Coble, P. G., Lead. J., Baker, A., Reynolds, D. M., and Spencer, R. G. M., Cambridge University Press, Cambridge, 75–122, Cambridge Books Online, doi:10.1017/CBO9781139045452, 2014.

Cole, J. J., Prairie, Y. T., Caraco, N. F., McDowell, W. H., Tranvik, L. J., Striegl, R. G., Duarte, C. M., Kortelainen, P., Downing, J. A., Middelburg, J. J., and Melack, J.: Plumbing the global carbon cycle: integrating inland waters into the terrestrial budget, Ecosystems, 10, 171–184, 2007.

Cory, R. M., Ward, C. P., Crump, B. C., and Kling, G. W.: Sunlight controls water column processing of carbon in arctic fresh waters, Science, 345, 925–928, 2014.

Crawley, M. J.: The R book, 2nd Edn., John Wiley & Sons, Chichester, 2012.

Del Giorgio, P. A., Cole, J. J., and Cimbleris, A.: Respiration rates in bacteria exceed phytoplankton production in unproductive systems, Nature, 385, 148–151, 1997.

Duarte, C. M. and Prairie, Y. T.: Prevalence of heterotrophy and atmospheric CO_2 emissions from aquatic ecosystems, Ecosystems, 8, 862–870, 2005. Fichot, C. G. and Miller, W. L.: An approach to quantify depth-resolved marine photochemical fluxes using remote sensing: application to carbon monoxide (CO) photoproduction, Remote Sens. Environ., 114, 1363–1377, 2010.

Gabor, R. S., Baker, A., McKnight, D. M., and Miller, M. P.: Fluorescence indices and their interpretation, in: Aquatic Organic Matter Fluorescence, edited by: Coble, P. G., Lead, J., Baker, A., Reynolds, D. M., and Spencer, R. G. M., Cambridge University Press, Cambridge, 303–338, Cambridge Books Online, doi:10.1017/CBO9781139045452, 2014.

Gao, H. and Zepp, R. G.: Factors influencing photoreactions of dissolved organic matter in a coastal river of the south-eastern United States, Environ. Sci. Technol., 32, 2940–2946, 1998.

Gonsior, M., Schmitt-Kopplin, P., and Bastviken, D.: Depth-dependent molecular composition and photoreactivity of dissolved organic matter in a boreal lake under winter and summer conditions, Biogeosciences, 10, 6945–6956, doi:10.5194/bg-10-6945-2013, 2013.

Granéli, W., Lindell, M., and Tranvik, L. J.: Photo-oxidative production of dissolved inorganic carbon in lakes of different humic content, Limnol. Oceanogr., 41, 698–706, 1996.

Hu, C., Muller-Karger, F. E., and Zepp, R. G.: Absorbance, absorption coefficient, and apparent quantum yield: a comment on common ambiguity in the use of these optical concepts, Limnol. Oceanogr., 47, 1261–1267, 2002.

Hughes, D. D., Holliman, P. J., Jones, T., and Freeman, C.: Temporal variations in dissolved organic carbon concentrations in upland and lowland lakes in North Wales, Water Environ. J., 27, 275–283, 2012.

Humborg, C., Mörth, C. M., Sundbom, M., Borg, H., Blenckner, T., Giesler, R., and Ittekkot, V.: CO_2 supersaturation along the aquatic conduit in Swedish watersheds as constrained by terrestrial respiration, aquatic respiration and weathering, Glob. Change Biol., 16, 1966– 1978, 2010.

Jankoswki, J. J., Kieber, D. J., Mopper, K.: Nitrate and nitrite ultraviolet actinometers. Photochem Photobiol, 70, 319-328, 1999.

Jankoswki, J. J., Kieber, D. J., Mopper, K., Neale, P. J.: Development and intercalibration of ultraviolet solar actonometers. Photochem Photobiol, 71, 431-440, 2000.

Johannessen, S. C. and Miller, W. L.: Quantum yield for the photochemical production of dissolved inorganic carbon in seawater, Mar. Chem., 76, 271–283, 2001.

Jonsson, A., Meili, M., Bergström, A. K., and Jansson, M.: Whole-lake mineralization of allochthonous and autochthonous organic carbon in a large humic lake (Örträsket, N. Sweden), Limnol. Oceanogr., 46, 1691–1700, 2001.

Kirk, J. T. O.: Absorption of light within the aquatic medium, in: Light and Photosynthesis in Aquatic Ecosystems, 3rd Edn., Cambridge University Press, Cambridge, 50–97, 2010.

Klemedtsson, L., Ernfors, M., Björk, R. G., Weslien, P., Rütting, T., Crill, P., and Sikström, U.: Reduction of greenhouse gas emissions by wood ash application to a *Picea abies* (L.) Karst. forest on a drained organic soil, Eur. J. Soil Sci., 61, 734–744, 2010.

Koehler, B., Landelius, T., Weyhenmeyer, G. A., Machida, N., and Trankvik, L. J.: Sunlight-induced carbon dioxide emissions from inland waters, Global Biogeochem. Cy., 28, 696–711, 2014.

Kothawala, D., Murphy, K., Stedmon, C., Weyhenmeyer, G., and Tranvik, L.: Inner filter correction of dissolved organic matter fluorescence, Limnol. Oceanogr.-Meth., 11, 616–630, 2013.

Lawaetz, A. J. and Stedmon, C. A.: Fluorescence intensity calibration using the Raman scatter peak of water, Appl. Spectrosc., 63, 936–940, 2009.

Lindell, M. L., Granéli, H. W., and Bertilsson, S.: Seasonal photoreactivity of dissolved organic matter from lakes with contrasting humic content, Can. J. Fish. Aquat. Sci., 57, 875–885, 2000.

Mayer, B. and Kylling, A.: Technical note: The libRadtran software package for radiative transfer calculations – description and examples of use, Atmos. Chem. Phys., 5, 1855–1877, doi:10.5194/acp-5-1855-2005, 2005.

Menzel, D. H. and Corwin, N.: The measurement of total phosphorus in seawater based on the liberation of organically bound fractions by persulphate oxidation, Limnol. Oceanogr., 10, 280–282, 1965.

Molot, L. A. and Dillon, P. J.: Photolytic regulation of dissolved organic carbon in northern lakes, Global Biogeochem. Cy., 11, 357–365, 1997.

Müller, R. A., Kothawala, D. N., Podgrajsek, E., Sahlée, E., Koehler, B., Tranvik, L. J., and Weyhenmeyer, G. A.: Hourly, daily and seasonal variability in the absorption spectra of chromophoric dissolved organic matter in a eutrophic, humic lake, J. Geophys. Res.-Biogeo., 119, 1985–1998, 2014.

Murphy, J. and Riley, J.: A single-solution method for the determination of soluble phosphate in seawater, J. Mar. Biol. Assoc. UK, 37, 9–14, 1958.

Murphy, K. R., Butler, K. D., Spemcer, R. G. M., Stedmon, C. A., Boehme, J. R., and Aiken, G. R.: Measurement of dissolved organic matter fluorescence in aquatic environments: an interlaboratory comparison, Environ. Sci. Technol., 44, 9405–9412, 2010.

Petrov, M., Terzhevik, A. Y., Palshin, N., Zdorovennov, V., and Zdorovennova, G.: Absorption of solar radiation by snow-and-ice cover of lakes, Water Resour., 32, 496–504, 2005.

Nelder, J. A. and Mead, R.: A simplex method for function minimization, Comput. J., 7, 308–313, 1965.

Rand, M., Greenberg, A., Taras, M. (Eds.): Standard Methods for the Examination of Water and Wastewater, American Public Health Association, Washington, 306–309, 1976.

Rundel, R. D.: Action spectra and estimation of biologically effective UV radiation, Physiol. Plantarum, 58, 360–366, 1983.

Ritz, C. and Streibig, J. C.: Nonlinear regression with R, 1st Edn., Springer-Verlag, New York, 2008.

Salonen, K. and Vähätalo, A.: Photochemical mineralisation of dissolved organic matter in Lake Skjervatjern, Environ. Int., 20, 307–312, 1994.

SMHI: Statistik: Isläggning och Islossning, available at: http://www.smhi.se/polopoly_fs/1.28756!/Statistik_isl%C3%A4ggning_och_islossning_2013.pdf (last access: 11 November 2014), 2013.

SMHI: Öppna Data, Meteorologiska Observationer, available at: http:// opendata-download-metobs.smhi.se/explore/ (last access: 21 January 2015), 2015.

Spencer, R. G. M., Hernes, P. J., Ruf, R., Baker, A., Dyda, R. Y., Stubbins, A., and Six, J.: Temporal controls on dissolved organic matter and lignin biogeochemistry in a pristine tropical river, Democratic Republic of Congo, J. Geophys. Res.-Biogeo., 115, G03013, doi:10.1029/2009JG001180, 2010.

Stubbins, A., Spencer, R. G., Chen, H., Hatcher, P. G., Mopper, K., Hernes, P. J., Mwamba, V. L., Mangangu, A. M., Wabakanghanzi, J. N., and Six, J.: 2010. Illuminated darkness: molecular signatures of Congo River dissolved organic matter and its photochemical alteration as revealed by ultrahigh precision mass spectrometry, Limnol. Oceanogr., 55, 1467–1477, 2010.

Suhett A. L., Amado A. M., Enrich-Prast A., Esteves F. A., Farjalla V. F. 2007 Seasonal changes of dissolved organic carbon photo-oxidation rates in a tropical lagoon: the role of rainfall as a major regulator. Can. J. Fish. Aquat. Sci. 64: 1266-1272.

Tranvik, L. J., Downing, J. A., Cotner, J. B., Loiselle, S. A., Striegl, R. G., Ballatore, T. J., Dillon, P., Finlay, K., Fortino, K., Knoll, L. B., Kortelainen, P. L., Kutser, T., Larsen, S., Laurion, I., Leech, D. M., McCallister, S. L., McKnight, D. M., Melack, J. M., Overholt, E., Porter, J. A., Prairie, Y., Renwick, W. H., Roland, F., Sherman, B. S., Schindler, D. W., Sobek, S., Tremblay, A., Vanni, M. J., Verschoor, A. M., von Wachenfeldt, E., and Weyhenmeyer, G. A.: Lakes and reservoirs as regulators of carbon cycling and climate, Limnol. Oceanogr., 54, 2298–2314, 2009.

Vachon, D., Lapierre, J.F., and del Giorgio, P. A.: Seasonality of photochemical dissolved organic carbon mineralization and its relative contribution to pelagic CO_2 production in northern lakes, J. Geophys. Res. Biogeosci., 121, 864–878, 2016.

Vähätalo, A. V., Salkinoja-Salonen, M., Taalas, P., and Salonen, K.: Spectrum of the quantum yield for photochemical mineralization of dissolved carbon in a humic lake, Limnol. Oceanogr., 45, 664–676, 2000.

Vähätalo, A. V. and Wetzel, R. G.: Photochemical and microbial decomposition of chromophoric dissolved organic matter during long (months–years) exposures, Mar. Chem., 89, 313–326, 2004.

Weishaar, J. L., Aiken, G. R., Bergamaschi, B. A., Fram, M. S., Fujii, R., Mopper, K.: Evaluation of specific ultraviolet absorbance as an indicator of the chemical composition and reactivity of dissolved organic carbon, Environ. Sci. Technol., 37, 4702–4708, 2003.

Zhang, Y., Xie, H., and Chen, G.: Factors affecting the efficiency of carbon monoxide photoproduction in the St. Lawrence estuarine system (Canada), Environ. Sci. Technol., 40, 7771–7777, 2006.

Ziegler, S. and Benner, R.: Effects of solar radiation in dissolved organic matter cycling in a subtropical seagrass meadow, Limnol. Oceanogr., 45, 257–266, 2000.

Tables

Table 1. Chemical and optical water properties of lake Erssjön during the study period of 2014

Month	DOC ($mg\ L^{-1}$)	TN ($mg\ L^{-1}$)	TP ($\mu g\ L^{-1}$)	pH	a_{254} (m^{-1})	a_{420} (m^{-1})	$SUVA_{254}$ ($L\ mg\ C^{-1}\ m^{-1}$)	FI	HIX	FRESH
April	18.8	NA	NA	5.5	210.5	21.0	11.2	NA	NA	NA
May	17.9	1.06	31	5.4	208.3	20.4	11.6	1.29	14.22	0.46
June	17.4	0.87	34	6.2	201.8	18.9	11.6	1.29	12.55	0.46
July	17.7	0.97	29	5.9	207.4	22.2	11.7	1.30	12.18	0.49
August	25.5	2.21	32	5.6	283.6	27.2	11.1	1.30	12.70	0.46
September	30.6	1.02	28	5.9	341.4	35.2	11.2	1.32	14.77	0.46
October	28.8	NA	33	5.0	309.3	28.7	10.7	1.33	14.86	0.47
November	NA	1.11	37	4.8	311.3	28.8	NA	1.32	13.60	0.46
Mean ± SE	22.4 ± 2.2	1.20 ± 0.2	32 ± 1	5.5 ± 0.2	251.7 ± 20.6	25.3 ± 2.0	11.3 ± 0.1	1.31 ± 0.01	13.55 ± 0.46	0.47 ± 0.004

DOC: dissolved organic carbon; TN: total nitrogen; TP: total phosphorus; a_{254}: absorption coefficient at 254 nm; a_{420}: absorption coefficient at 420 nm; $SUVA_{254}$: specific UV absorption coefficient at 254 nm; FI: fluorescence index; HIX: humification index; FRESH: freshness index.

Table 2. Mean (± SE) background variables (n=8 in 2012 and 2014, n=12 in 2013), and simulated irradiance and photochemical DIC production rates assuming lowest (left) and highest (right) photochemical reactivity measured in 2014.

	2012		2013		2014	
DOC (mg L^{-1})	23.5 ± 1.6*		21.1 ± 0.4		22.4 ± 2.2#	
a_{420} (m^{-1})	25.8 ± 3.0		20.3 ± 0.8		25.3 ± 2.0	
$SUVA_{254}$ (L mg C^{-1} m^{-1})	10.2 ± 0.3*		10.1 ± 0.2		11.3 ± 0.1#	
Irradiance (Wh m^{-2} yr^{-1})	$3.88 \cdot 10^5$		$4.19 \cdot 10^5$		$4.18 \cdot 10^5$	
DIC_{areal} (mg C m^{-2} d^{-1})	7.2 ± 0.3	35.5 ± 1.5	8.2 ± 0.3	43.3 ± 1.7	8.3 ± 0.4	45.0 ± 1.9
Range	0.3 – 19.3	1.7 – 102.8	0.3 – 19.7	2.1 – 102.7	0.3 – 20.0	1.6 – 111.3
DIC_{areal} (g C m^{-2} yr^{-1})	1.8	8.9	2.0	10.8	2.1	11.2
DIC_{lake} (kg C yr^{-1})	126.8	625.3	143.5	762.0	146.5	791.7

DOC: dissolved organic carbon; a_{420}: absorption coefficient at 420 nm; $SUVA_{254}$: specific UV absorption coefficient at 254 nm; Irradiance: irradiance integrated over the wavelength range 280-600 nm; DIC_{areal} and DIC_{lake}: areal and total lake DIC photoproduction rate simulated for the open water season, 249 days between the average ice-off and ice-on dates; * n=6; # n=7.

Table 3. Mean (± SE) photochemical DIC production under the full irradiance spectrum in the solar simulator, and absorbed photons as well as the total AQY in the wavelength range 280-600 nm; parameter estimates for the fitted AQY spectra (eq. 2), information on performance to reproduce the observations (R^2, regression slope and nRMSE) and areal photochemical DIC production in 2014 using the respective AQY spectra. Values in parentheses give diagnostics and simulation results when single AQY spectra were used to predict photochemical DIC production observed during all six irradiation experiments

AQY	DIC production under full irradiance (μmol L^{-1} h^{-1})	CDOM-absorbed $photons_{280-600}$ (mol m^{-2} h^{-1})	AQY_{total} (mmol DIC mol $photons^{-1}$)	m_1	m_2
June	9.28 ± 0.72	3.12 ± 0.23	0.138 ± 0.003	$5.776^{+0.518}_{-0.429}$	$0.032^{+0.007}_{-0.007}$
July	7.54 ± 0.42	3.77 ± 0.26	0.093 ± 0.006	$5.985^{+0.373}_{-0.454}$	$0.033^{+0.006}_{-0.004}$
August	17.57 ± 0.90	3.97 ± 1.81	0.206 ± 0.007	$5.846^{+0.156}_{-0.168}$	$0.023^{+0.002}_{-0.002}$
September	19.90 ± 1.26	4.52 ± 0.31	0.204 ± 0.004	$5.839^{+0.137}_{-0.166}$	$0.022^{+0.001}_{-0.001}$
October	29.41 ± 1.76	4.02 ± 0.28	0.341 ± 0.016	$5.782^{+0.282}_{-0.316}$	$0.018^{+0.003}_{-0.003}$
November	33.87 ± 0.98	4.21 ± 0.24	0.375 ± 0.014	$5.967^{+0.176}_{-0.218}$	$0.015^{+0.002}_{-0.002}$
monthly measured	NA	NA	NA	NA	NA
pooled	NA	NA	NA	$6.350^{+0.672}_{-0.639}$	$0.017^{+0.006}_{-0.005}$

Table 3. *Continued.*

AQY	R^2	slope	nRMSE (%)	DIC_{areal} (g C m^{-2} yr^{-1})
June	0.98 (0.58)	1.03 (0.32)	5.89 (25.91)	(3.0)
July	0.96 (0.57)	0.99 (0.24)	7.27 (28.94)	(2.2)
August	0.99 (0.60)	1.01 (0.55)	3.35 (17.42)	(5.8)
September	0.99 (0.60)	1.01 (0.60)	3.42 (16.87)	(6.4)
October	0.97 (0.60)	1.01 (0.87)	5.71 (24.67)	(10.1)
November	0.99 (0.61)	1.01 (0.92)	4.30 (30.94)	(12.2)
monthly measured	NA	NA	NA	(3.9)
pooled	(0.61)	(0.52)	(16.97)	(7.3)

AQY: apparent quantum yield; DIC: dissolved inorganic carbon; CDOM: chromophoric dissolved organic matter; AQY_{total}: DIC production measured under full irradiance (280 nm filter) divided by CDOM-absorbed photons integrated from 280 to 600 nm; m_1 and m_2: fit parameters with 95% confidence intervals; R^2 and slope: R^2 and slope of a linear regression between observed and predicted DIC photoproduction; nRMSE: normalised root mean squared error between observed and predicted DIC photoproduction; DIC_{areal}: areal DIC photoproduction rate simulated for the open water season of 2014, 310 days between the ice-off and ice-on dates.

Figure legends

Figure 1. a: Map of Sweden showing the location of lake Erssjön (blue star). b: Aerial photo of lake Erssjön, indicating the locations of the two floating frames used during in situ measurement of DIC photoproduction (red dots) and the location of the flux chambers (white dots) (image obtained from Google maps; Imagery ©2015 Lantmäteriet/Metria, Map data ©2015 Google). c: Floating frame with the quartz and control tubes positioned at three different water depths.

Figure 2. Apparent quantum yield (AQY) spectra for a. June, b: July, c: August, d: September, e: October, and f: November, including simultaneous pointwise 95% confidence intervals at 295, 330, 365, 400 and 435 nm. For comparison, the AQY spectra of the other months are added in grey in each panel.

Figure 3. Photochemical DIC production rates observed in situ (± SE; black numbers) and simulated using photochemical rate modelling (red curve and average values over the intended depths of the experimental tubes). The frame to which the tubes were attached sank into the sediment by about 1 cm during the two incubation days. Simulated values adjusted to this change in incubation depths are given in parentheses.

Figure 4. a: Daily irradiance integrated over the wavelength range 280-600 nm. b: Daily photochemical DIC production rate from 2012 to 2014 using the AQY spectrum with highest (November; primary y-axis) and the lowest productivity (July; secondary y-axis) measured in 2014. The grey shaded areas mark the ice-covered periods of the lake, during which we set DIC photoproduction to zero assuming no irradiance transmission (Petrov et al., 2005).

Figure 5. Box-and-whiskers plots of total measured CO_2 emissions, and minimum and maximum simulated photochemical DIC production, showing the median and 1st and 3rd quartiles with the whiskers set at ±1.5 times the interquartile range and data outside this range

given as circles. Note the log scale on the y-axis.

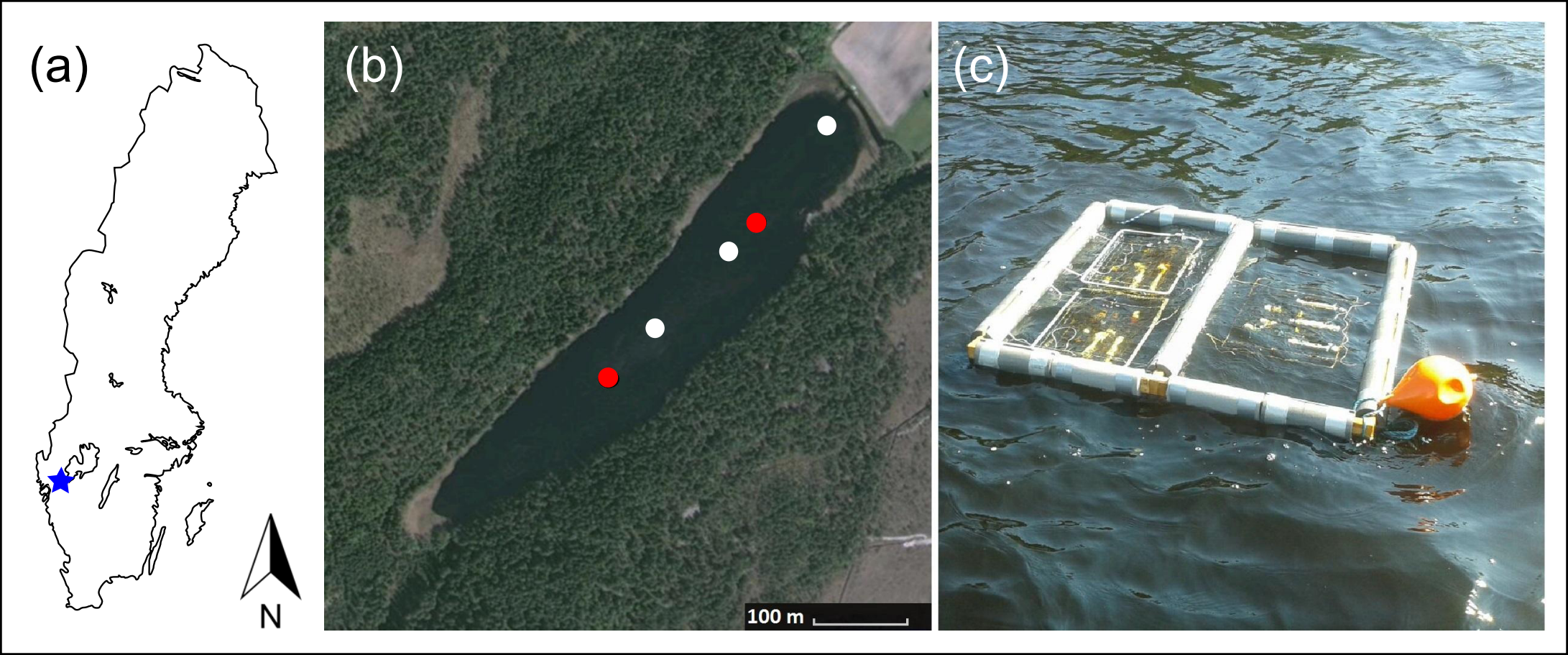
(a)
N
(b)
100 m
(c)

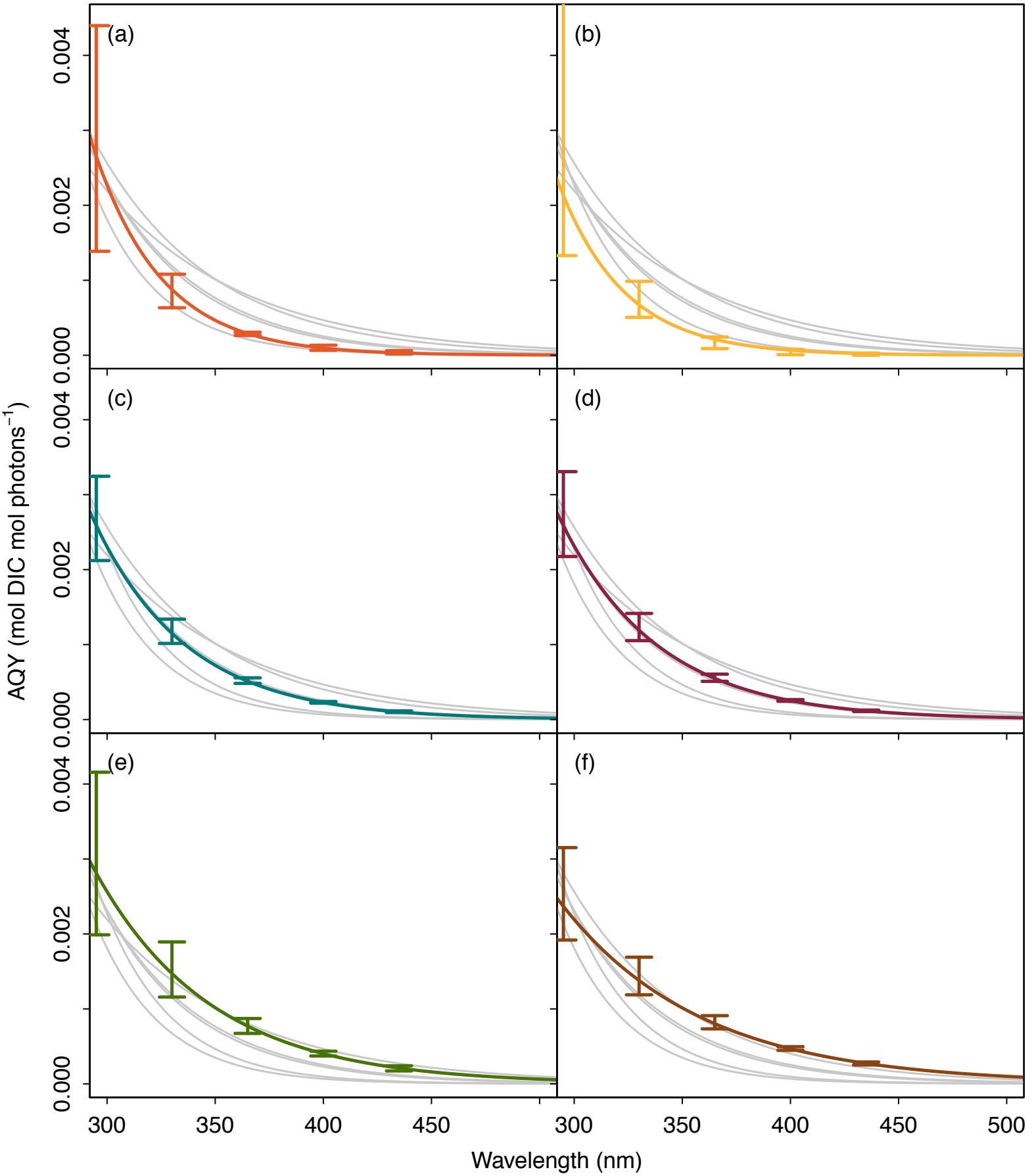
(a)
(b)
(c)
(d)
(e)
(f)
AQY (mol DIC mol photons^{-1})
0.000
0.002
0.004
300
350
400
450
500
Wavelength (nm)

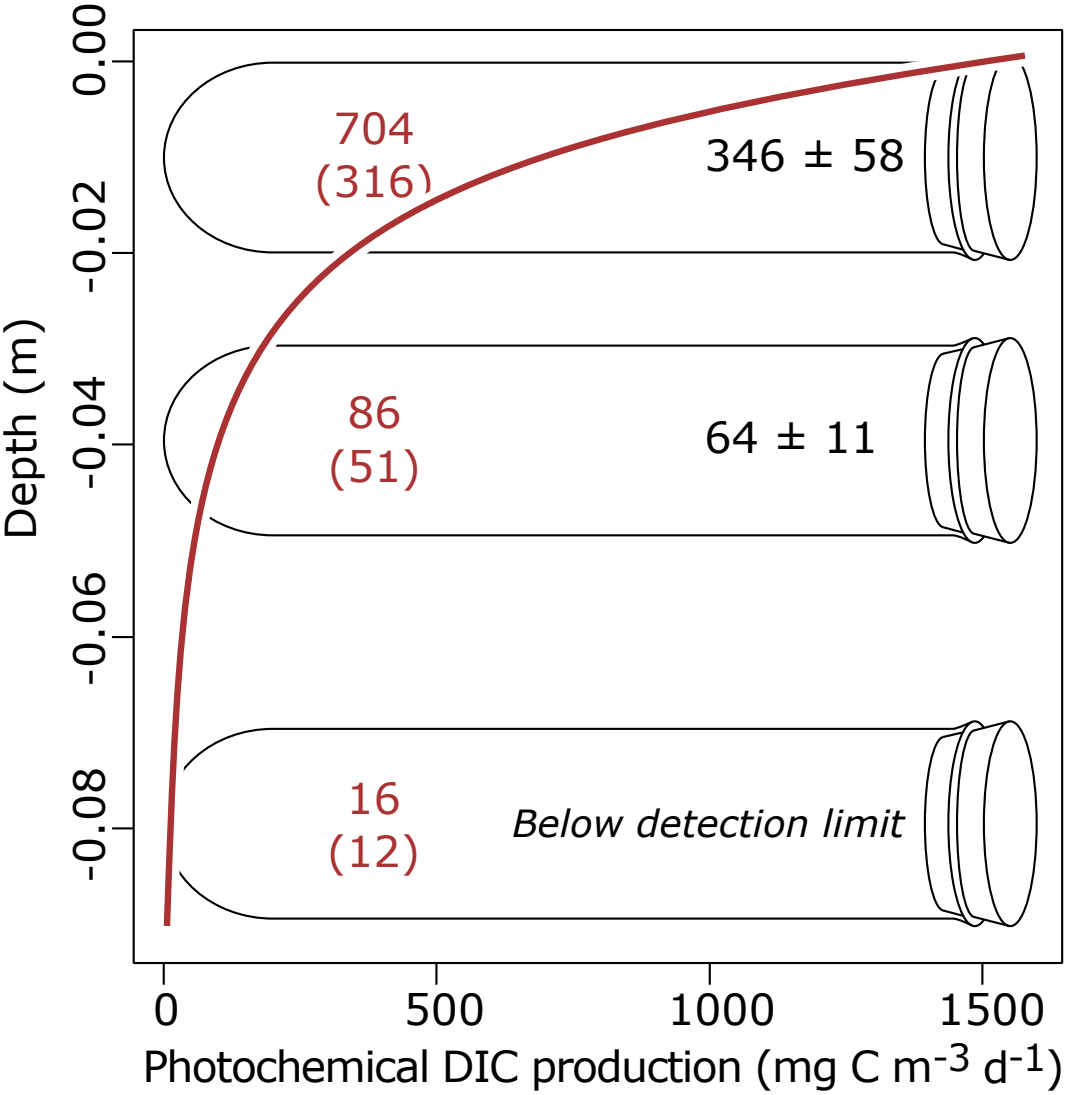
Depth (m)
0.00
-0.02
-0.04
-0.06
-0.08
704
(316)
346 ± 58
86
(51)
64 ± 11
16
(12)
Below detection limit
0
500
1000
1500
Photochemical DIC production (mg C m-3 d-1)

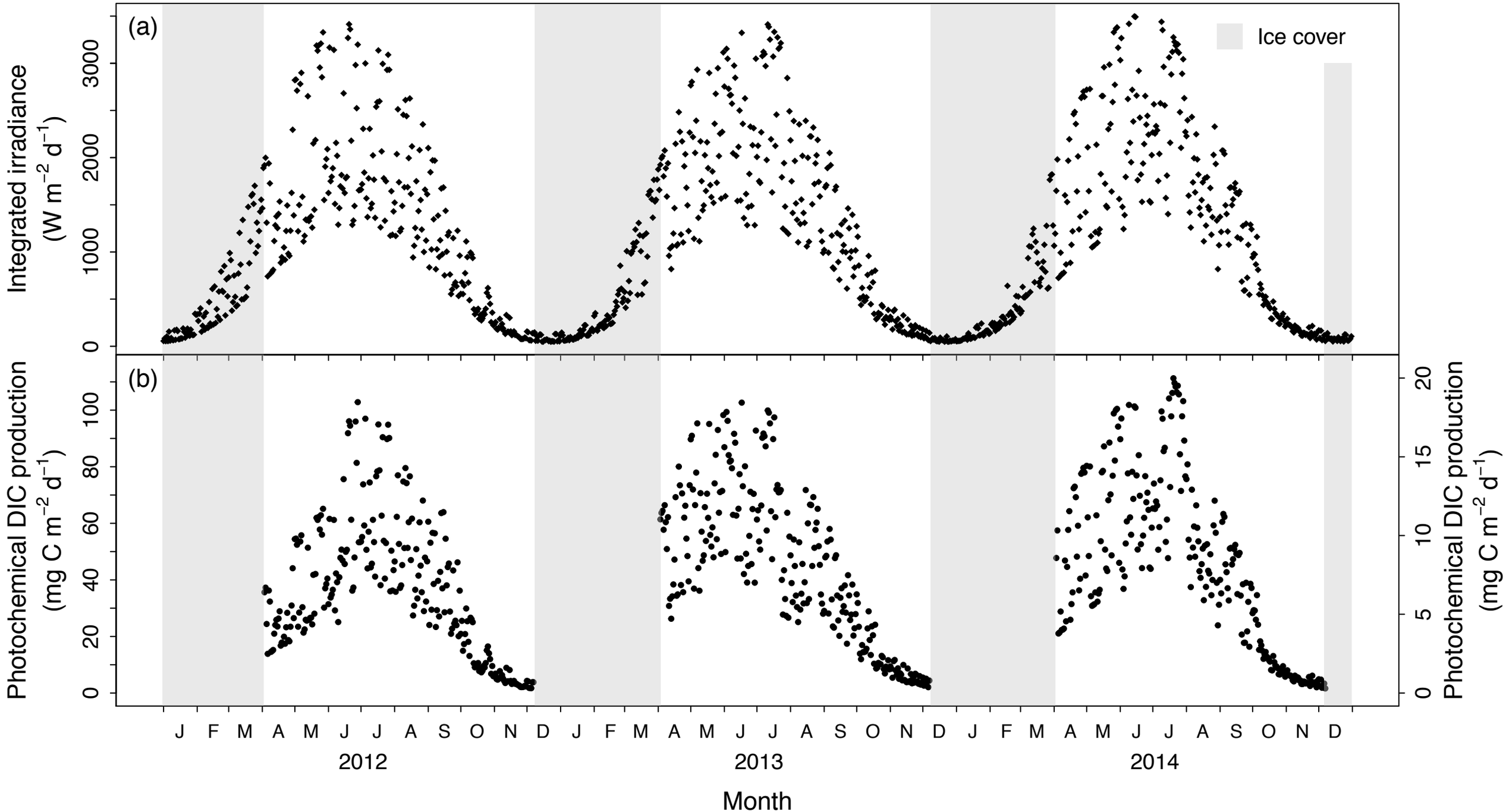
(a)
Ice cover
Integrated irradiance
(W m^{-2} d^{-1})
0
1000
2000
3000
(b)
Photochemical DIC production
(mg C m^{-2} d^{-1})
0
20
40
60
80
100
0
5
10
15
20
J F M A M J J A S O N D J F M A M J J A S O N D J F M A M J J A S O N D
2012
2013
2014
Month

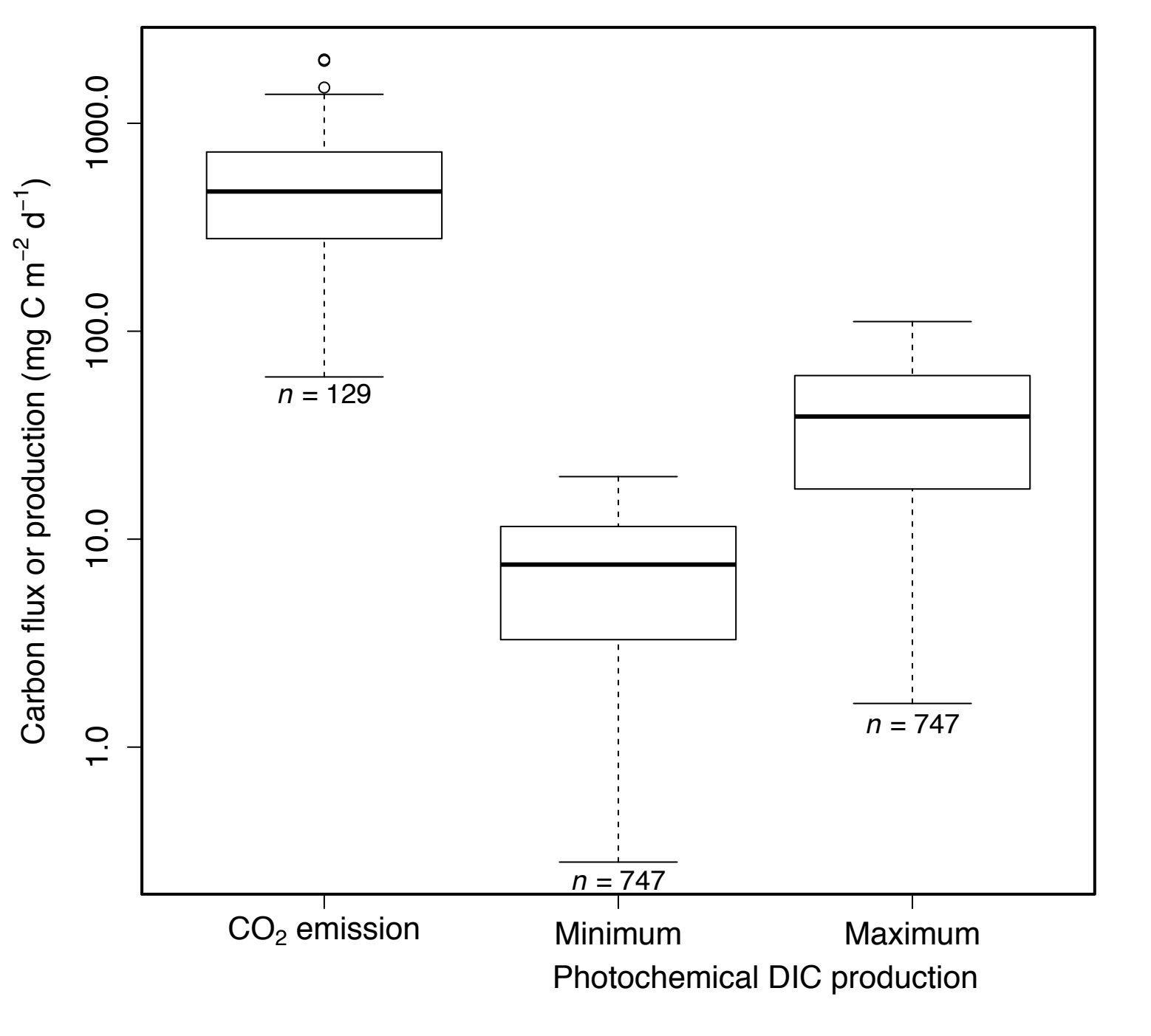
Carbon flux or production (mg C m^{-2} d^{-1})
1000.0
100.0
10.0
1.0
n = 129
n = 747
n = 747
CO2 emission
Minimum
Maximum
Photochemical DIC production